This article has been accepted for publication in IEEE Transactions on Industry Applications. This is the author's version which has not been fully edited and content may change prior to final publication. Citation information: DOI 10.1109/TIA.2022.3190241

Improvement of the Distribution Systems Resilience via Operational Resources and Demand Response

Juan M. Home-Ortiz, Ozy D. Melgar-Dominguez, Mohammad S. Javadi, *Senior Member, IEEE*, José Roberto Sanches Mantovani, *Member, IEEE*, and João P. S. Catalão, *Fellow, IEEE*

***Abstract*—This work presents a restoration approach for improving the resilience of electric distribution systems (EDSs) by taking advantage of several operational resources. In the proposed approach, the restoration process combines dynamic network reconfiguration, islanding operation of dispatchable distributed generation (DG) units, and the pre-positioning and displacement of mobile emergency generation (MEG) units. The benefit of exploring a demand response (DR) program to improve the recoverability of the system is also taken into account. The proposed approach aims to separate the in-service and out-of-service parts of the system while maintaining the radiality of the grid. To assist the distribution system planner, the problem is formulated as a stochastic scenario-based mixed-integer linear programming model, where uncertainties associated with PV-based generation and demand are captured. The objective function of the problem minimizes the amount of energy load shedding after a fault event, as well as PV-based generating curtailment. To validate the proposed approach, adapted 33-bus and 83-bus EDSs are analyzed under different test conditions. Numerical results demonstrate the benefits of coordinating the dynamic network reconfiguration, the pre-positioning and displacement of MEG units, and a DR program to improve the restoration process.**

Keywords—Demand response, dynamic reconfiguration, islanding DG operation, mobile emergency generators, resilience, restoration.

NOMENCLATURE

Indices:

c	Index for operational scenario
$i/j/n$	Index for nodes
ij	Index for branches
st	Index for staging locations
t	Index for periods
y	Index for linearization blocks

Sets:

Γ_B	Set of branches
Γ_B^*	Set of branches including both directions ij and ji
Γ_G	Set of nodes with dispatchable distributed generators
Γ_H	Set of artificial branches
Γ_N	Set of nodes
Γ_N^I	Set of nodes that were not affected by the fault
Γ_M	Set of candidate nodes to install MEG units
Γ_{PV}	Set of nodes with PV-based generation
Γ_S	Set of substation nodes
Γ_{ST}	Set of staging locations
Γ_C^t	Set of scenarios of period t
Γ_T	Set of periods
Γ_U	Set of MEG units. $\Gamma_U = \{1, 2, \ldots, k_{st}^{MEG}\}$

Parameters:

c_i^{LS}	Cost of the load shedding at node i
c_i^{PV}	Cost of PV-based power generation curtailment
C_i^C	Connection time of a MEG unit at node i
R_{ij}, X_{ij}, Z_{ij}	Resistance/reactance/magnitude of the impedance of a branch
$\overline{I}_{ij}$	Current capacity limit of a branch
k_{st}^{MEG}	Number of MEG units available at the staging location st
$\underline{V}$, $\overline{V}$	Minimum/maximum voltage magnitudes
$P_{i,t,c}^D$	Active power demand
$\overline{P}^{MEG}$	Active power limit of the MEG units
P_i^{PVins}	Installed PV-based generation capacity
$\overline{S}_i^{DG}$	Apparent power capacity of a DG unit
$T_{st,i}^{CT}$, $T_{st,i}^{TT}$	Congestion traffic time and elapsed time of the displacement of a MEG unit from the staging location st to node i
V_i^{DG}	Voltage nominal of a dispatchable DG unit
$\overline{S}_{ij}^S$	Apparent power capacity of a substation
Y	Number of discrete blocks used in the linearization of the current calculation
δ_i	Demand response limit
Δ_t	Period duration
$\rho_{t,c}$	Scenario probability
σ_i^D	Demand power factor
$\underline{\sigma}_i$, $\overline{\sigma}_i$	Limit for capacitive/inductive power factors of a DG unit

Continuous variables:

$I_{ij,t,c}^{SQ}$	Square of the current magnitude
$P_{ij,t,c}$, $Q_{ij,t,c}$	Active/reactive power flows
$P_{i,t,c}^{DG}$, $Q_{i,t,c}^{DG}$	Active/reactive power generations of a dispatchable DG unit
$P_{i,t,c}^{DR}$, $Q_{i,t,c}^{DR}$	Active/reactive power demand considering demand response program
$P_{i,t,c}^{MEG}$, $Q_{i,t,c}^{MEG}$	Active/reactive power generations of a mobile emergency generation unit
$P_{i,t,c}^{PV}$	Active power generation of a PV-based generation unit
$P_{i,t,c}^{curt}$	Active power curtailment of a PV-based generation unit
$P_{i,t,c}^S$, $Q_{i,t,c}^S$	Active/reactive power generations at a substation
$T_{st,i,n}^{xMEG}$	Traveling time by n MEG units
$V_{i,t,c}^{SQ}$	Square of the voltage magnitude

This work was supported in part by the São Paulo Research Foundation (FAPESP) under Grants 2019/01841-5, 2019/23755-3, 2018/12422-0 and 2015/21972-6, in part by the Coordination for the Improvement of Higher Education Personnel (CAPES) finance code 001, in part by the Brazilian National Council for Scientific and Technological Development (CNPq) under Grant 304726/2020-6, and in part by FEDER funds through COMPETE 2020 and by Portuguese funds through FCT, under POCI-01-0145-FEDER-029803 (02/SAICT/2017). Mohammad S. Javadi acknowledges FCT for his contract funding provided through 2021.01052.CEECIND.

J.M. Home-Ortiz, O.D. Melgar-Dominguez and J.R.S. Mantovani are with the Department of Electrical Engineering São Paulo State University (UNESP) Ilha Solteira, São Paulo, Brazil. (e-mail: juan.home@unesp.br, ozy.daniel@unesp.br, and mant@dee.feis.unesp.br)

M.S. Javadi is with the INESC TEC, Porto, 4200-465, Portugal (e-mail: msjavadi@gmail.com).

J.P.S. Catalão is with the Faculty of Engineering of the University of Porto and INESC TEC, Porto, 4200-465, Portugal (e-mail: catalao@fe.up.pt).

$v_{ij,t,c}$, $v_{i,t,c}^{DG}$	Slack voltage variables
Binary variables:	
$u_{i,n,t}^{MEG}$	Defines the n MEG units connected at node i and period t
$w_{ij,t}$	Status of a switch at period t
$x_{i,t}$	Defines the in-service or out-of-service status of the demand at node i, at period t
$z_{st,i,n}^{MDG}$	Indicates the displacement of the MEG unit n from the staging location st to node i
$\beta_{ij,t}$	Auxiliary variable used in the radiality constraints.

I. Introduction

Electric distribution systems (EDSs) are planned, operated, and controlled to provide an economical, safe, and reliable energy supply to passive and active users. However, the EDS infrastructure could be vulnerable when some extreme and rare incidents occur. Under this scenario, these events denoted as High-Impact and Low-Probability (HILP) events, result in extended outages and negative economic impacts, being necessary to incorporate their effects into the strategies for the expansion planning and operation of EDSs [1]. In this context, distribution system operators (DSOs) are paying more attention to leveraging the implementation of operational resources to improve the EDS recoverability and mitigate the negative effects due to emergency conditions [2].

In order to face multiple outages caused by extreme events, reference [3] develops a strategy to sectionalize the on-outage area by forming microgrids, and re-dispatching of existing distributed generation (DG) units, for which the service is recovered to affected users. Similarly, the authors in [4] propose a strategy to optimize the coordination of energy storage systems to improve the EDS recoverability. Once existing resources are exploited, the DSO can manage other options to optimize the service restoration. For example in [5], a strategy that coordinates the operation of repair crews and emergency mobile DG units is presented. The authors in [6], present a multi-decision framework that employs switching actions and defines the most suitable locations for positioning mobile emergency generation (MEG) units to speed up post-disturbance actions. Other methodologies have been explored not only the occurrence of extreme events, but also traffic congestions in the problem formulation as proposed in [7].

However, modeling the real-world transportation network increases the problem formulation complexity, thus becoming necessary the implementation of simplification techniques to consider network transportation effects in resilience studies [8]. In [9], a simulation-assisted mixed-integer linear programming (MILP) model is proposed for resilience enhancement of distribution systems, where dynamic network reconfiguration and microgrid formation are considered in the restoration process. In [10], a two-stage stochastic scenario-based MILP model is proposed for resilience enhancement of distribution system, where the first stage also pre-allocates MEG units and other available resources, and the second stage generates the intraday operation decisions.

On the other hand, demand response (DR) is an essential operational resource that can benefit both users and the DSO. Within a range of load variations, this program provides the flexibility to change demand patterns according to the received signal due to incentives and/or disincentives that promote the interaction and responsiveness between the users and the DSO [11]. It is known that the inclusion of DR, into the resilience problems, enables a reduction of the total number of switching operations, and can increase the total amount of demand restored [12]. In [13] an approach is proposed to take advantage of different resources, including a DR program for resilience analysis, where it is observed that controlling some loads can assist the DSO to improve the system operation in the recovery stage. Similarly, [14] investigates that a DR program can significantly improve the EDS recoverability even when limited DG and microgrids face multiple outages. The authors in [15] propose a two-stage strategy that determines, in the first stage, the network reconfiguration while the second stage defines the restored critical loads, the optimal DG units dispatch, and the output of responsive loads.

In modern EDSs, the recoverability process faces new challenges due to the high shares of renewable-based DG technologies. To assess such impacts, reference [16] presents a probabilistic event model, where the time-varying dependencies of renewable-based DG output and load characteristics are captured while a set of metrics are quantified to determine the EDS resilience. In [17], multiple operational resources are coordinated to deal with emergency conditions, where impacts of renewable-based DG and demand response programs are also evaluated. Similarly, the authors in [18] formulate a strategy to enhance the operational resilience to damage caused by windstorms, by considering not only uncertainties of renewable-based power productions, but also uncertainties in wind speed that can affect the most vulnerable EDS branches.

This condition gives rise to developing new strategies, considering several challenges and possibilities in order to obtain more resilient EDSs. Although there is a considerable number of strategies to face multiple outages caused by HILP events, the complexity of the problem, considering several operational resources is accentuated, being necessary to develop more robust strategies to improve the restoration process in EDSs. Therefore, this work presents a significantly extended version of [19], where the problem is formulated from the DSO perspective and a novel strategy to simultaneously coordinate several operational resources is designed to improve the recoverability of an EDS after the occurrence of HILP events. The strategy is formulated as a stochastic MILP model, where the objective function minimizes the total non-restored energy and the generation curtailment of renewable-based DG along the operation period. This strategy should coordinate the operation of resources such as topology reconfiguration, islanding DG operation, and dispatching of emergency mobile DG units. In addition, the impacts of increasing penetration of renewable-based DG and the benefits of a DR program are taken into account. Contrasted with existing approaches, the main contributions of this work can be highlighted as follows:

1) Proposing a multitemporal resilience-based strategy to tackle the recoverability problem after the occurrence of a set of HILP fault events in an EDS. The problem is formulated from the perspective of the DSO and

consists of coordinating simultaneously several operational resources to face, in the most suitable way, emergency conditions. The operational resources include the dynamic network reconfiguration, microgrid formation, displacement and operation of MEG units, and the possibility to explore the flexibility of a DR program, where demand patterns can be modified to improve the EDS recoverability. In addition, the effects of high shares of renewable-based DG penetration from the point of view of a resilient system are considered in the problem formulation.

2) Developing a MILP model for formulating the resilience problem that guarantees finite convergence using commercial optimization solvers. This MILP model can be explored as an efficient tool to assist the DSO in the decision-making process by generating a set of possible actions to improve the EDS operation under emergency conditions.

This work is structured as follows: Section II presents the MILP formulation of the problem; Section III presents the obtained results and discussion for a multiple fault scenario in a 33-node and 83-node EDSs; finally, conclusions are drawn in Section IV.

II. Mathematical model

In this section, the resilience problem under analysis is formulated as a stochastic MILP model. The formulation considers several operational resources such as the dynamic radial reconfiguration, islanding operation, dispatchable DG, mobile emergency generators, and a DR program. It is also assumed that a high penetration level of PV-based DG is placed in the EDS; thus, after an occurrence of a HILP event, the proposed strategy should improve the EDS recoverability.

A. Objective function

The objective function $\mathcal{F}$, presented in (1) minimizes the total nonrestored energy and the generation curtailment of PV-based DG along the operation day Γ_T.

minimize $\mathcal{F}$:

$$\sum_{t\in\Gamma_T}\sum_{c\in\Gamma_C^t}\rho_{t,c}\Delta_t\left(\sum_{i\in\Gamma_N}c_i^{LS}P_{i,t,c}^{D}x_{i,t}+c_i^{PV}\sum_{i\in\Gamma_{PV}}P_{i,t,c}^{PVcurt}\right) \tag{1}$$

The first sum quantifies the total nonrestored load without considering the demand at the faulted section according to the status of the binary variable $x_{i,t}$. Therefore, if $x_{i,t}=1$, then node i is not restored at period t and the value of the objective function increases; otherwise, if $x_{i,t}=0$, node i is connected to the system. The second sum penalizes the total generation curtailment of PV-based DG. In the proposed formulation, the restoration process can prioritize the recovering of critical nodes by considering different values of the load shedding cost, c_i^{LS}.

B. Network model

For all the periods Γ_T and stochastic scenarios Γ_C^t, the constraints (2)–(6) represent the power flow calculation while constraints (7)–(10) represent the EDS operational limits.

$$P_{i,t,c}^{S}+P_{i,t,c}^{DG}+P_{i,t,c}^{MEG}+P_{i,t,c}^{PV}+\sum_{ji\in\Gamma_B}P_{ji,t,c}-\sum_{ij\in\Gamma_B}\left(P_{ij,t,c}+R_{ij}I_{ij,t,c}^{SQ}\right)=P_{i,t,c}^{DR} \tag{2}$$

$$Q_{i,t,c}^{S}+Q_{i,t,c}^{DG}+Q_{i,t,c}^{MEG}+\sum_{ji\in\Gamma_B}Q_{ji,t,c}-\sum_{ij\in\Gamma_B}\left(Q_{ij,t,c}+X_{ij}I_{ij,t,c}^{SQ}\right)=Q_{i,t,c}^{DR} \tag{3}$$
$$\forall(i\in\Gamma_N,t\in\Gamma_T,c\in\Gamma_C^t)$$

$$V_{j,t,c}^{SQ}I_{ij,t,c}^{SQ}=P_{ij,t,c}^{2}+Q_{ij,t,c}^{2} \tag{4}$$

$$V_{i,t,c}^{SQ}-V_{j,t,c}^{SQ}+v_{ij,t,c}=2\left(R_{ij}P_{ij,t,c}+X_{ij}Q_{ij,t,c}\right)+Z_{ij}^{2}I_{ij,t,c}^{SQ} \tag{5}$$

$$\left|v_{ij,t,c}\right|\le\left(\overline{V}^{2}-\underline{V}^{2}\right)\left(1-w_{ij,t}\right) \tag{6}$$
$$\forall(ij\in\Gamma_B,t\in\Gamma_T,c\in\Gamma_C^t)$$

$$0\le I_{ij,t,c}^{SQ}\le\overline{I}_{ij}^{2}w_{ij,t}\qquad\forall(ij\in\Gamma_B,t\in\Gamma_T,c\in\Gamma_C^t) \tag{7}$$

$$\left|P_{ji,t,c}\right|\le\overline{VI}_{ij}w_{ij,t}\qquad\forall(ij\in\Gamma_B,t\in\Gamma_T,c\in\Gamma_C^t) \tag{8}$$

$$\left|Q_{ji,t,c}\right|\le\overline{VI}_{ij}w_{ij,t}\qquad\forall(ij\in\Gamma_B,t\in\Gamma_T,c\in\Gamma_C^t) \tag{9}$$

$$\underline{V}^{2}\le V_{i,t,c}^{SQ}\le\overline{V}^{2}\qquad\forall(i\in\Gamma_N,t\in\Gamma_T,c\in\Gamma_C^t) \tag{10}$$

Constraints (2) and (3) represent the active and reactive power flow balance at nodes. While (4)–(6) determine the voltage drop calculation according to the operation state of branch ij which is defined by the binary variable $w_{ij,t}$. Constraint (4) determines the square of the current through the branches. The voltage-drop between node i and node j is determined in (5), in this constraint, the slack variable $v_{ij,t,c}$ allows the voltage drop calculation when the branch ij is open. In this regard, according to (6), if branch ij is close $\left(w_{ij,t}=1\right)$, then $v_{ij,t,c}$ is 0, otherwise, it is limited by $\left(\overline{V}^{2}-\underline{V}^{2}\right)$. Constraints (7)–(9) define the current, active, and reactive power flow through branches, while constraint (10) imposes the voltage limits. Quadratic constraint (4) is linearized using the piecewise linear approximation technique presented in [20]. Details of the linearization are presented in the Appendix section. Constraints (11)–(13) represent the operational limits of dispatchable DG units.

$$0\le P_{i,t,c}^{DG}\le\overline{S}_i^{DG} \tag{11}$$

$$-\overline{S}_i^{DG}\le Q_{i,t,c}^{DG}\le\overline{S}_i^{DG} \tag{12}$$

$$-\left(\sqrt{2}\,\overline{S}_i^{DG}-P_{i,t,c}^{DG}\right)\le Q_{i,t,c}^{DG}\le\left(\sqrt{2}\,\overline{S}_i^{DG}-P_{i,t,c}^{DG}\right) \tag{13}$$
$$\forall(i\in\Gamma_G,t\in\Gamma_T,c\in\Gamma_C^t)$$

Constraints (11)–(13) represent a linearization of the capability curve of the synchronous machine that is normally represented as a quadratic constraint $(\bar{S}^2\ge P^2+Q^2)$. Constraints (11) and (12) determine the active and reactive power limit of the DG. Constraint (13) is a tangent cut used to improve the approximation of the capability curve of the machine.

Similar to (11)–(13), constraints (14)–(16) represent a linearization of the operational limits of the substations.

$$0\le P_{i,t,c}^{S}\le\overline{S}_i^{S} \tag{14}$$

$$-\overline{S}_i^{S}\le Q_{i,t,c}^{S}\le\overline{S}_i^{S} \tag{15}$$

$$-\left(\sqrt{2}\,\overline{S}_i^{S}-P_{i,t,c}^{S}\right)\le Q_{i,t,c}^{S}\le\left(\sqrt{2}\,\overline{S}_i^{S}-P_{i,t,c}^{S}\right) \tag{16}$$
$$\forall(i\in\Gamma_S,t\in\Gamma_T,c\in\Gamma_C^t)$$

In the substation nodes, constraint (14) defines the active power limit, while constraints (15) and (16) determine the reactive power limits.

Operational constraints for the PV-based DG are presented in (17) and (18).

$$0\le P_{i,t,c}^{PV}=P_i^{PVins}\left(1-x_{i,t}\right)-P_{i,t,c}^{PVcurt} \tag{17}$$

This article has been accepted for publication in IEEE Transactions on Industry Applications. This is the author's version which has not been fully edited and content may change prior to final publication. Citation information: DOI 10.1109/TIA.2022.3190241

$$0 \le P_{i,t,c}^{curt} \le P_i^{PVins}\left(1 - x_{i,t}\right) \quad \forall(i \in \Gamma_{PV}, t \in \Gamma_T, c \in \Gamma_C^t) \tag{18}$$

Constraint (17) defines the power injected by the PV-based units according to the power capacity and the active power curtailment which is limited in (18) to the available power.

C. Demand response model

In this paper, the power demand after the fault event is modeled using a DR program that consists of a predefined mutual agreement between the DSO and end-users. Under this agreement, the end-users (or a group of them) are willing to make available a percentage of manageable demand that the DSO can manage to comply with technical constraints under normal and emergency conditions.

$$\sum_{t\in\Gamma_T} P_{i,t,c}^{DR}\Delta_t \ge \sum_{t\in\Gamma_T}\left(P_{i,t,c}^{D}\Delta_t\left(1 - x_{i,t}\right)\right) \quad \forall(i \in \Gamma_N, c \in \Gamma_C) \tag{19}$$

$$P_{i,t,c}^{D}(1-\delta_i)\left(1 - x_{i,t}\right) \le P_{i,t,c}^{DR} \le P_{i,t,c}^{D}(1+\delta_i)\left(1 - x_{i,t}\right) \tag{20}$$

$$Q_{i,t,c}^{DR} = P_{i,t,c}^{DR}\tan\left(\cos^{-1}\left(\sigma_i^D\right)\right) \quad \forall(i \in \Gamma_N, t \in \Gamma_T, c \in \Gamma_C^t) \tag{21}$$

In this formulation, parameter $P_{i,t,c}^{D}$ defines the load profile of the node before the fault event. Constraint (19) defines that, under emergency conditions, the energy demand at in-service/restored node i is at least equal to the energy demand profile of the node before the fault event, i.e., under normal operational conditions. Constraint (20) defines the range for the DR program following a load profile including the load shedding integer variable $x_{i,t}$ in the DR program model. Finally, constraint (21). determines the reactive power demand following the active power demand variations considering a constant power factor $\sigma_i^D = \frac{P_i^D}{\sqrt{\left(P_i^D\right)^2 + \left(Q_i^D\right)^2}}$, where P_i^D and Q_i^D are the active and reactive nominal load at node i under normal conditions, respectively.

D. Mobile emergency generation units

To enhance the restoration process, the optimal scheduling of MEG units is considered through the mathematical formulation (22)–(30). This formulation considers the optimal traveling time, connection point, number of units that are required, and operation. When a fault occurs, the DSO can send MEG units from the staging location, st, to a new location i.

$$\sum_{i\in\Gamma_N^{MDG}}\sum_{n=1}^{\bar{n}} z_{st,i,n}^{MEG} \le k_{st}^{MEG} \quad \forall(st \in \Gamma_{ST}) \tag{22}$$

$$z_{st,i,n}^{MEG} \le z_{st,i,n-1}^{MEG} \quad \forall(st \in \Gamma_{ST}, i \in \Gamma_M, n \in \Gamma_U) \tag{23}$$

$$T_{st,i,n}^{xMEG} = \left(T_{st,i}^{CT}T_{st,i}^{TT} + C_i^C\right)z_{st,i,n}^{MEG} \quad \forall(t \in \Gamma_{ST}, i \in \Gamma_M, n \in \Gamma_U) \tag{24}$$

$$\sum_{t\in\Gamma_T} t\, r_{i,n,t}^{MEG} \ge \sum_{st\in\Gamma_{st}} T_{st,i,n}^{xMEG} \quad \forall(i \in \Gamma_M, n \in \Gamma_U) \tag{25}$$

$$\sum_{t\in\Gamma_T} t\, r_{i,n,t}^{MEG} \le \sum_{st\in\Gamma_{st}} T_{st,i,n}^{xMEG} \quad \forall(i \in \Gamma_M, n \in \Gamma_U) \tag{26}$$

$$\sum_{t\in\Gamma_T} r_{i,n,t}^{MEG} = \sum_{st\in\Gamma_{st}} z_{st,i,n}^{MEG} \quad \forall(i \in \Gamma_M, n \in \Gamma_U) \tag{27}$$

$$u_{i,n,t^*}^{MEG} = \sum_{t\in\Gamma_T} r_{i,n,t}^{MEG} \quad \forall(i \in \Gamma_M, n \in \Gamma_U, t^* \in \Gamma_T | t < t^*) \tag{28}$$

$$0 \le P_{i,t,c}^{MEG} \le \overline{P}^{MEG}\sum_{n=1}^{\bar{n}} u_{i,n,t}^{MEG} \quad \forall\begin{pmatrix} i \in \Gamma_M, n \in \Gamma_U, \\ t \in \Gamma_T, c \in \Gamma_C^t \end{pmatrix} \tag{29}$$

$$P_{i,t,c}^{MEG}\tan\left(\cos^{-1}\left(\underline{\sigma}^{MDG}\right)\right) \le Q_{i,t,c}^{MEG} \le P_{i,t,c}^{MEG}\tan\left(\cos^{-1}\left(\overline{\sigma}^{MDG}\right)\right) \quad \forall\begin{pmatrix} i \in \Gamma_M, n \in \Gamma_U, \\ t \in \Gamma_T, c \in \Gamma_C^t \end{pmatrix} \tag{30}$$

Constraint (22) determines that the total number of required units to be connected to the system does not exceed the number of available MEG units. Auxiliary constraint (23) imposes a sequence on the units to be sent to node i. Constraint (24) stablishes the necessary traveling time ($T_{st,i}^{xMEG}$) to send a MEG unit from the staging location "*st*" to be connected at node i. The traveling time is defined by the elapsed time ($T_{st,i}^{TT}$) between two points, *st* and i, affected by the time demanded due road congestions ($T_{st,i}^{CT}$) and the necessary time (C_i^C) to connect the MEG unit at location i. For determining the time *t* when a MEG unit is connected to the location i, constraints (25) and (26) are used that directly associate *t* with the $T_{st,i}^{xMEG}$. Constraint (27) is used to couple the binary variables that model the MEG units sent to new locations $z_{st,i,n}^{MEG}$ and the auxiliary variable $r_{i,n,t}^{MEG}$ that estimate their connection time.

In this formulation, it is considered that MEG units can only carry out one travel. To guarantee it, constraint (28) ensures that once a MEG unit arrives and is connected at node i, this unit remains installed for the subsequent periods. The active and reactive power limits of the MEG unit are defined by (29) and (30), respectively.

E. Network topology constraints

This subsection presents the topology constraints used to restore the system after a fault event including the topological separation between in-service and out-of-service nodes, radial network reconfiguration, and radial islanding operation with master/slave DG operation. These possibilities and conditions can be achieved through two fictitious substation nodes S1 and S2, as proposed in [19]. Under emergency conditions, a master unit is a dispatchable DG with black start capability that provides voltage reference to the restored system while renewable generators operate always as slave units.

The first fictitious substation node S1 is used to solve the problem of separating in-service and out-of-service nodes. This substation uses a fictitious grid (Γ_H) to be directly connected to each EDS node i.e., there is a fictitious path between each node of the real system and S1, as presented in Fig. 1 (a). Thus, after the restoration process, the out-of-service parts of the system stay connected to this substation. On the other hand, the fictitious substation node S2 is used to solve the master/slave operation of the DG units. This substation uses a set of extra open fictitious switches which are within the set of branches Γ_B, to connect with the DG units that can operate as master units, as presented in Fig. 1 (a). Then, if one of these switches is closed, its respective DG unit is operating as a master unit i.e., operating as the reference node in its island.

For illustrative purposes, Fig. 1 presents the proposed radial restoration process with islanding operation. In Fig. 1 (a), it is shown a distribution system with five nodes and one substation in normal operation, where the DG units, G1 and G2, are operating as slave units; moreover, fictitious substations S1 and S2 are presented. In Fig. 1 (b), it is displayed a fault at branch 2-3 affecting nodes 3, 4, and 5.

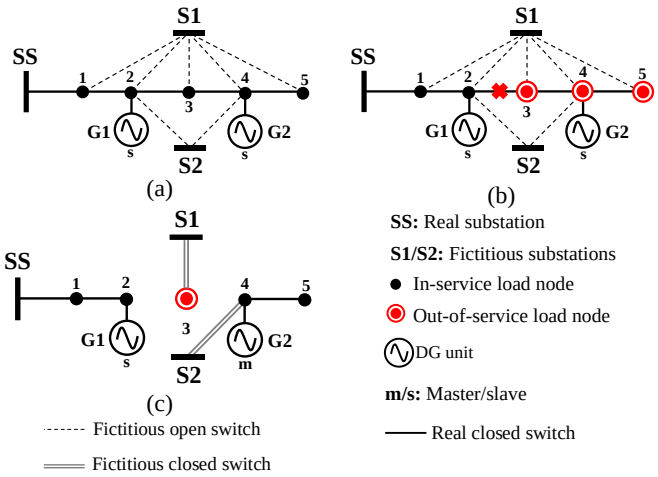

Figure 1. Radial restoration process with islanding operation

Finally, in Fig. 1 (c) the G2 unit is connected to the fictitious substation S2, and the out-if-service node 3 is connected to the fictitious substation S1. Then, the unit G1 continues operating as a slave unit; the unit G2 is operating in islanded operation as a master unit providing power balance to nodes 4 and 5, while node 3 cannot be restored. In this case, the DG unit G2 has no capacity to provide power to node 3.

For each period, the radiality constraints (31)–(33) represent the network as an expansion tree according to the operating state of the branches avoiding the loop formation and the interconnection between substation nodes [21]. These constraints guarantee that the DG master units cannot be connected with other substations or with other DG master units. These constraints include real and fictitious grids.

$$\beta_{ij,t} + \beta_{ji,t} = w_{ij,t} \qquad \forall(ij \in \Gamma_B \cup \Gamma_H, t \in \Gamma_T) \qquad (31)$$

$$\sum_{ij \in \Gamma_B^*} \beta_{ij,t} = 1 \qquad \forall(i \in \Gamma_N \cup \Gamma_H, t \in \Gamma_T | i \notin \Gamma_S) \qquad (32)$$

$$\beta_{ij,t} = 0 \qquad \forall(ij \in \Gamma_B^*, t \in \Gamma_T | i \in \Gamma_S) \qquad (33)$$

Constraint (31) is used to determine the direction of the connection of the expansion tree according to the status of the branch ij. In this constraint, in a period t, $\beta_{ij,t}$=1, indicates a connection between nodes i and j in the direction $j \rightarrow i$ considering a substation as root node.

Constraint (32) ensures the connectivity of the system with the substation nodes, it includes real and fictitious substation nodes. Constraint (33) avoids the loop formation by fixing at zero the $\beta_{ij,t}$ variables that indicate an entry direction at substation nodes.

To separate the in-service and the out-of-service parts of the system, constraint (34) imposes that a branch only can connect two nodes if they have the same operational status, i.e., $x_{i,t} = x_{j,t}$. Constraint (35) avoids the disconnection of nodes that were not affected by the fault, and constraint (36) avoids the disconnection of in-service nodes during the restoration process.

$$|x_{i,t} - x_{j,t}| \leq (1 - w_{ij,t}) \qquad \forall(ij \in \Gamma_B, t \in \Gamma_T) \qquad (34)$$

$$x_{i,t} = 0 \qquad \forall(i \in \Gamma_N^I, t \in \Gamma_T) \qquad (35)$$

$$x_{i,t} \leq x_{i,t-1} \qquad \forall(i \in \Gamma_N, t \in \Gamma_T | t \geq 1) \qquad (36)$$

According to the operational state of the DG units with black start capability, constraints (37)–(39) define the voltage of these devices.

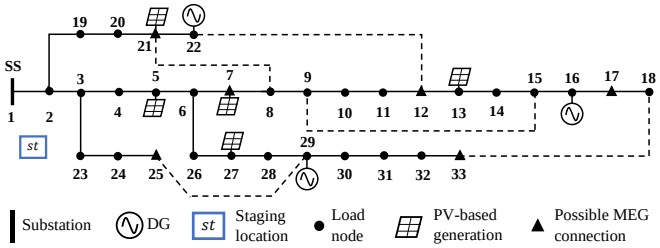

Figure 2. Normal operation of the 33-node system

$$V_{i,t,c}^{SQ} + v_{i,t,c}^{DG} = \left(V_i^{DG}\right)^2 \qquad \forall(i \in \Gamma_G, t \in \Gamma_T, c \in \Gamma_C^t) \qquad (37)$$

$$\left|v_{j,t,c}^{DG}\right| \leq \left(\overline{V}^2 - \underline{V}^2\right)(1 - w_{ij,t}) \qquad \forall\begin{pmatrix} ij \in \Gamma_B, t \in \Gamma_T, \\ c \in \Gamma_C^t | j \in \Gamma_G \wedge i \in \Gamma_S \end{pmatrix} \qquad (38)$$

$$w_{ij,t} = w_{ij,t-1} \qquad \forall\begin{pmatrix} ij \in \Gamma_B, t \in \Gamma_T \\ | j \in \Gamma_G \wedge t \geq 1 \end{pmatrix} \qquad (39)$$

Constraint (37) fixes the voltage at nodes with DG master units. Constraint (38) determines the slack variable $v_{i,t,c}^{DG}$ according with the status of the branch ij that connect it to substation node S2. If branch ij is close, then the DG unit at node i is selected as a master unit, the slack variable $v_{i,t,c}^{DG} = 0$, and the voltage at node i is fixed at V_i^{DG}. Finally, according to (39), the status of the DG units must remain the same over the restoration process.

III. Tests and Results

The performance and robustness of the proposed model are tested and analyzed using an adapted 33-node system from [22] presented in Fig. 2, and to validate its scalability the adapted 83-node system [23], presented in Fig. 3, is used. This section presents the technical information, assumptions, and case studies, to validate the proposed approach.

A. The 33-node System

The 33-node system, presented in Fig. 2, has one staging location with a capacity of five MEG units of 0.25 MVA with a power factor of 0.8, and nodes 7, 12, 17, 21, 25, and 33 are candidate locations to install up to 5 MEG units. The DR program considers that all the load nodes can modify up to ± 10% from the pre-fault consumption behavior. The available DG of the system is composed of three dispatchable DG that can operate as master units at nodes 16, 22, and 29 with capacities of 1.00, 0.75, and 0.75 MVA, respectively, and a power factor of 0.8.

Meanwhile, the PV-based DG is located at nodes 5, 7, 13, 21, and 27, where each unit has an installed capacity of 1.0 MW. In normal operation conditions, all the PV-based DG units have no generation curtailment, in other words, all the power production from these renewable energy sources is injected into the EDS. For this system, the proposed model is solved for a simultaneous fault at branches 2-3, 7-8, 15-16, and 24-25, this is a fault scenario where only 12.38% of the load remains in service.

B. The 83-node System

The 83-node system, presented in Fig. 3, has two staging locations with a capacity of 3 MEG units of 0.5 MVA with a

This article has been accepted for publication in IEEE Transactions on Industry Applications. This is the author's version which has not been fully edited and content may change prior to final publication. Citation information: DOI 10.1109/TIA.2022.3190241

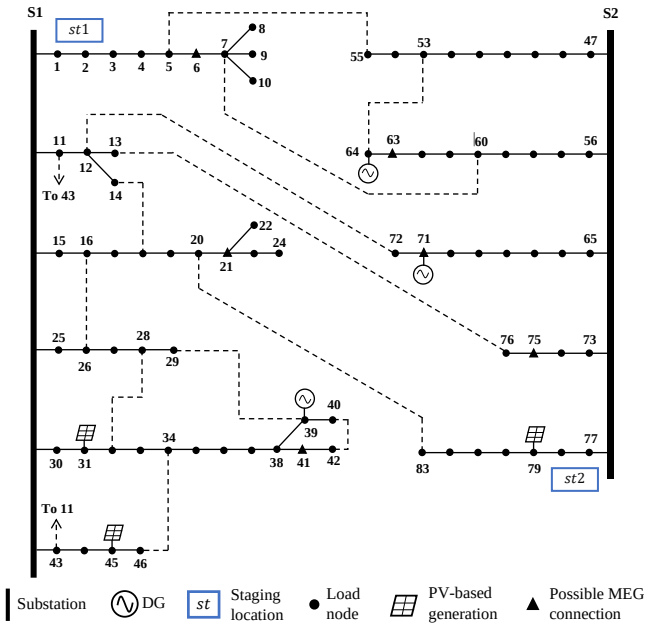

Figure 3. Normal operation of the 83-node system

power factor of 0.8. Nodes 6, 21, 41, 63, 71, and 75, are selected as candidate locations to install up to 2 MEG units for each node. All nodes of the system allow to modify up to ±10% of their demand, participating in the DR program. The system has three dispatchable DG units located at nodes 39, 71, and 64 with capacities of 5.0 MVA, 5.0 MVA, and 2.5 MVA, respectively. PV-based DG units are located at nodes 31, 45, and 79 with a total capacity of 3.0 MW. For test purposes here, the original demand obtained from [23] is increased by 30% of the nominal value. For this system, simulations are carried out considering a simultaneous fault at branches S1-15, S1-25, S1-30, S1-43, S2-47, S2-77, S2-73, and S2-65. This fault scenario affects 73.40 % of the power demand of the system.

C. Assumptions and case studies

For both test systems, variability and uncertainties in demand consumption and solar irradiation are considered through twelve times periods, where each time involves two stochastic scenarios. These scenarios are generated from historical data and reduced using the scenario reduction technique k-means [24].

Since the load has different levels in each period, it is worth mentioning that the percent of the in-service and out-of-service load presented in this paper are calculated considering a full demand scenario.

The restoration process is carried out for the following cases:

- Case I: This case considers all the possibilities in the restoration process, i.e., islanding operation, scheduling of MEG units, and DR program.
- Case II: In this case, the option of a DR program is disregarded.
- Case III: The restoration process disregards the option of dispatching MEG units.
- Case IV: Finally, DR program and the scheduling of MEG units are not considered for this analysis.

For comparative purposes, these cases are studied under dynamic and non-dynamic switching operations.

The optimization model was implemented in AMPL and solved with the commercial optimization solver CPLEX 20.1.0, and the numerical experiments have been conducted on a computer with a 2.8 GHz Intel® Core™ i7-7700HQ processor and 16 GB of RAM.

D. Results for the 33-node System

1). Numerical results considering dynamic network reconfiguration.

This subsection presents the obtained results considering dynamic topology reconfiguration.

In this condition, Fig. 4 presents the percentage of in-service active load during the restoration process for Cases I-IV.

In addition, Table I presents the open and closed switches for each period, the scheduling of MEG units indicating the connection node and the traveling time in hours, and the dispatchable DG units that were selected as master units. Table II presents the generation curtailment in each PV-based DG unit. It is worth noting that in these cases, all the proposed solutions have the same dispatchable DG units operating in islanding operations.

Case I: In this case, the restoration process consists of a solution that at period t_0 has an in-service load of 66.62%, at period t_1 it increases up to 69.85%, and, at period t_4 the in-service load is 75.24% remaining until the end of the analysis. The dynamic topology reconfiguration process is composed of 8 switching operations at period t_0, one closing operation at period t_1, one more closing operation at period t_4. Finally, this solution has two MEG units connected at note 7, with an arriving time of 2.13h.

Case II: When the option of a DR program is not available, the restoration process has three stages with in-service loads of 65.01, 68.24, and 73.62%, respectively. The first stage needs 7 switching operations at period t_0, the second one requires two switching operations at period t_1, and one close switching operation at period t_4. Analogously to Case I, two MEG units are sent to node 7 with a traveling time of 2.13h. The PV generation curtailment at node 5 is not calculated since this node is out-of-service throughout all the periods. Compared with the previous case, disregarding the DR program represents a drop of 1.61% of the in-service load in all the periods.

Case III: Disregarding the MEG units scheduling, the restoration process only presents switching operations in period 0 and the total in-service active load is 63.93% for all the periods. In this case, the dynamic reconfiguration of the network cannot increase the amount of in-service load even with the option of a DR program.

Case IV: As shown in Case III, the restoration process has switching operations only in period 0, however, the amount of in-service active load is 62.31% for all the periods. This result shows that considering the DR program is possible to increase the amount of in-service active load by 1.62%. As node 5 is out-of-service in all the periods, then it is not possible to determine its PV generation curtailment.

This article has been accepted for publication in IEEE Transactions on Industry Applications. This is the author's version which has not been fully edited and content may change prior to final publication. Citation information: DOI 10.1109/TIA.2022.3190241

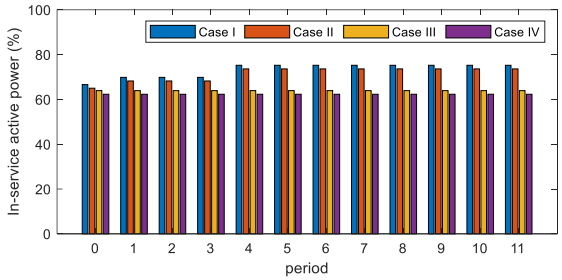

Figure 4. In-service active power considering dynamic switching operation for the 33-node system.

TABLE I
RESTORATION PROCESS OF THE 33-NODE SYSTEM CONSIDERING DYNAMIC SWITCHING OPERATIONS

Case	Open switches	Closed switches	MEG dispatch	Master DG units
I	t_0(4-5, 6-7, 6-26, 29-30, 30-31)	t_0(12-22, 18-33, 25-29); t_1(6-26); t_4(6-7)	st →7(2.13h); st →7(2.13h)	16, 29
II	t_0(6-7, 26-27, 29-30, 30-31); t_1(5-6)	t_0(12-22, 18-33, 25-29); t_1(26-27); t_4(6-7)	st →7(2.13h); st →7(2.13h)	16, 29
III	t_0(4-5, 29-30, 30-31)	t_0(12-22, 18-33)	–	16, 29
IV	t_0(5-6, 12-13, 29-30, 30-31)	t_0(9-15, 12-22, 18-33)	–	16, 29

TABLE II
PV-BASED GENERATION CURTAILMENT (MWH) OF THE 33-NODE SYSTEM CONSIDERING DYNAMIC SWITCHING OPERATIONS

Node	Case I	Case II	Case III	Case IV
5	2.8940	-	4.2333	-
7	0.7718	1.1126	1.9888	2.2694
13	0.0698	0.1272	0.0698	0.5752
21	0.2164	0.4818	0.2164	0.0338
27	0.0000	0.0000	1.6302	1.8783

Obtained results reveal that in cases where MEG units were considered, cases I and II, it is possible to increase the amount of in-service load throughout the periods. However, in cases where the MEG units were disregarded, cases III and IV, the in-service load remains constant during all periods.

It is worth noting that the solution obtained for the case I presents the most appropriate resilience plan, where negative impacts on the power production of PV-based DG are minimized, in other words, less generation was curtailed compared to solutions of Cases II-IV.

2). Numerical results without dynamic network reconfiguration.

In this subsection, the Cases I-IV are presented disregarding the possibility of dynamic reconfiguration. i.e., switching operations are allowed only in period 0. This condition limits the restoration capacity of the system throughout the day; thus, the total in-service load during and after the restoration process remains constant for all periods.

Case I: In this case, after the restoration process, 67.70% of the active load is in-service. The restoration process consists of three switching operations, two MEG units, and one dispatchable DG in the islanding operation. In this case, node 5 cannot be restored, then its PV generation curtailment is not determined.

TABLE III
RESULTS OF THE 33-NODE SYSTEM WITHOUT DYNAMIC SWITCHING OPERATIONS

Case	Open switches	Closed switches	MEG dispatch	Master DG units
I	t_0(5-6);	t_0(12-22, 18-33)	st →7(2.13h); st →7(2.13h)	16
II	t_0(4-5, 29-30, 30-31)	t_0(12-22, 18-33)	st →7(2.13h)	16, 29
III	t_0(4-5, 29-30, 30-31)	t_0(8-21, 18-33)	–	16, 29
IV	t_0(5-6, 29-30, 30-31)	t_0(12-22, 18-33)	–	16, 29

TABLE IV
PV-BASED ENERGY CURTAILMENT (MWH) OF THE 33-NODE SYSTEM WITHOUT DYNAMIC SWITCHING OPERATIONS

Node	Case I	Case II	Case III	Case IV
5	-	4.3441	4.2333	-
7	0.0000	2.2694	1.9888	2.2694
13	0.0698	0.1272	0.0698	0.1272
21	0.2164	0.4818	0.2164	0.4818
27	0.0000	1.8783	1.6302	1.8783

Case II: Disregarding the DR program, the restoration process needs seven switching operations, one MEG unit, and two DGs operating in islanding operation to reach a configuration with an in-service active load of 63.93%.

Case III: Despite the MEG units being disregarded, in this case, the DR program allows the system to have a total in-service active load equal to Case II with the same network topology.

Case IV: This case presents the same topology as Cases II and III, however, the total in-service active load is 62.31%. Similar to Case I, node 5 remains out-of-service, then the PV generation curtailment is not calculated.

E. Results for the 83-node System

The 83-node system [23] is used to validate the scalability of the proposed approach solving systems with more than one substation. This subsection presents the obtained results for cases I-IV considering and disregarding dynamic switching operation.

1). Numerical results considering dynamic network reconfiguration

Considering the 83-nodes system, Fig. 5 shows the amount of in-service active load during the restoration process for Cases I-IV. Details of the restoration process are presented in Table V including the switching operations for each period, the dispatch of MEG units indicating the staging location, connection node, the traveling time in hours, the number of MEG units installed, and the dispatchable DG units that were selected as master units. For all the cases, in the obtained solutions the dispatchable DG units operate in slave mode. Moreover, the restored systems have 0.00% of PV-based generation curtailment at node 45, while only nodes 31 and 79 cannot be restored.

Case I: Considering all the alternatives, the restoration process consists of a multi-step solution that at period t_0 has an in-service load of 72.66%, at period t_{10} it increases up to 82.54%, and at period t_{11} the in-service active load is 84.13%. The dynamic topology reconfiguration process is composed of 13 opening switching operations and 16 closing operations. Finally, this solution requires four MEG units, two units connected at note 71 and two units connected at

This article has been accepted for publication in IEEE Transactions on Industry Applications. This is the author's version which has not been fully edited and content may change prior to final publication. Citation information: DOI 10.1109/TIA.2022.3190241

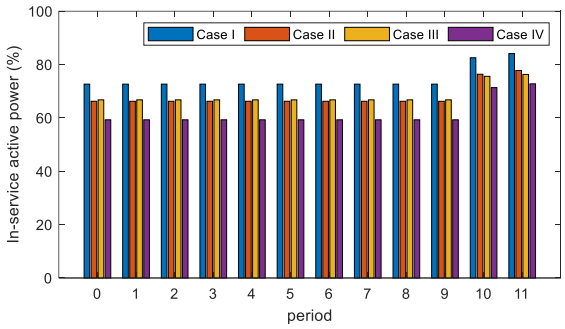

Figure 5. In-service active power considering dynamic switching operation for the 83-node system.

TABLE V
RESTORATION PROCESS OF THE 83-NODE SYSTEM CONSIDERING DYNAMIC SWITCHING OPERATIONS

Case	Open switches	Closed switches	MEG dispatch	Master DG units
I	t_0(6-7, 18-19, 26-27, 27-28, 31-32, 38-41, 41-42, 53-54); t_{10}(20-21, 37-38, 79-80); t_{11}(21-22, 23-24)	t_0 (5-55, 7-60, 11-43, 12-72, 13-76, 14-18, 16-26, 20-83, 29-39, 34-46, 40-42, 53-64); t_{10} (18-19, 26-27, 27-28); t_{11} (20-21)	st_1 →71(3.59h); st_1 →71(3.59h); st_2 →75(3.26h); st_2 →75(3.26h)	X
II	t_0(6- 7, 18-19, 25-26, 32-33, 36-37, 37-38, 50-51, 53-54, 68-69, 75-76); t_{10}(19-20, 31-32); t_{11}(66-67)	t_0(5-55, 7-60, 11-43, 12-72, 13-76, 14-18, 16-26, 29-39, 34-46, 53-64); t_{10}(18-19, 25-26, 37-38, 50-51, 75-76, 28-32); t_{11}(68-69)	st_1 →71(3.59h); st_1 →71(3.59h); st_2 →41(4.75h); st_2 →63(2.17h)	X
III	t_0(6-7, 18-19, 26-27, 27-28, 32-33, 39-40, 49-50, 53-54, 68-69, 75-76); t_{10}(19-20, 35-36); t_{11}(31-32);	t_0(5-55, 7-60, 11-43, 12-72, 13-76, 14-18, 16-26, 29-39, 34-46, 53-64) t_{10}(18-19, 26-27, 27-28, 75-76) t_{11}(32-33)	–	X
IV	t_0(6-7, 18-19, 31-32, 33-34, 38-39, 41-42, 45-46, 51-52, 69-70, 75-76); t_2(67-68); t_{10}(37-38)	t_0(7-60, 11-43, 12-72, 13-76, 14-18, 16-26, 28-32, 29-39, 34-46, 40-42, 53-64); t_{10}(45-46, 51-52, 75-76); t_{11}(69-70)	–	X

node 75, with arriving times of 3.59h and 3.26h, respectively.

Case II: Disregarding the DR program during the restoration process, the solution of the problem proposes a restoration process that at period t_0 has an in-service active load of 66.24% that increases up to 76.37% at period t_{10}, and at period t_{11} is 77.78%. The proposed solution is based on 13 opening switching operations and 17 closing switching operations. In this case, four MEG units distributed among nodes 71, 41, and 63 are connected to the system.

Case III: When MEG units are not available to be connected to the system, the restoration process consists of a solution that at period t_0 has an in-service load of 66.77%, and at period t_{10} it increases up to 75.59% and at period t_{11} increases again up to 76.30%. The dynamic network reconfiguration process is composed of 13 opening and 15 closing switching operations.

TABLE VI
RESTORATION PROCESS OF THE 83-NODE SYSTEM WITHOUT DYNAMIC SWITCHING OPERATION

Case	Open switches	Closed switches	MEG dispatch	Master DG units
I	t_0(6- 7, 18-19, 25-26, 31-32, 38-41, 63-64)	t_0(5-55, 7-60, 11-43, 12-72, 13-76, 16-26, 29-39, 34-46, 53-64)	st_1 →71(3.59h); st_1 →71(3.59h); st_2 →75(3.26h); st_2 →75(3.26h)	X
II	t_0(6- 7, 18-19, 25-26, 32-33, 39-40, 50-51, 53-54, 68-69, 75-76)	t_0(5-55, 7-60, 11-43, 12-72, 13-76, 14-18, 16-26, 29-39, 53-64)	st_1 →71(3.59h); st_1 →71(3.59h); st_2 →41(4.75h); st_2 →63(2.17h)	X
III	t_0(6-7, 18-19, 32-33, 35-36, 37-38, 63-64, 70-71, 75-76)	t_0(5-55, 7-60, 11-43, 12-72, 13-76, 14-18, 16-26, 29-39, 34-46, 53-64)	–	X
IV	t_0(6-7, 18-19, 31-32, 33-34, 38-39, 41-42, 45-46, 51-52, 70-71, 75-76)	t_0(7-60, 11-43, 12-72, 13-76, 14-18, 16-26, 28-32, 29-39, 40-42, 53-64)	–	X

Case IV: Disregarding the DR program and the MEG units during the restoration process, the solution of the problem has an in-service load of 59.29% at period t_0 that increases at period t_{10} up to 71.36%, and at period t_{11} reaches 72.77%. The dynamic network reconfiguration process is composed of 12 opening and 15 closing switching operations.

By analyzing the obtained results, the restoration process that considers all the possibilities, Case I, has the best performance, since the in-service load at period t_{11} is 6.35%, 7.83%, and 11.36% higher when compared to Cases II-IV, respectively. For this system, dynamic network reconfiguration allows increasing the amount of in-service load through periods in all the cases.

2). Numerical results without dynamic network reconfiguration.

In this subsection, the obtained solutions for cases I-IV disregarding the possibility of dynamic reconfiguration are presented. Details of the restoration process are presented in Table VI including the switching network topology, scheduling of MEG units indicating the pre-positioned staging location, connection node, traveling time in hours, the number of MEG units installed per node, and the islanding operation of dispatchable DG units. Under these conditions, the dispatchable DG units are operating in slave mode in all cases, moreover, the restored system has zero percent of PV-based generation curtailment at node 45 while nodes 31 and 79 cannot be restored.

Case I: By considering a DR program and MEG units during the restoration process, 72.66% of the active load is in-service. The restoration process consists of 15 switching operations and four MEG units, where are distributed and

connected at nodes 71 and 75.

Case II: Disregarding the DR program, the restoration process requires 18 switching operations and four MEG units, where two MEG units are connected at node 71, and two at nodes 41 and 63. This solution reaches an in-service active load of 66.24%.

Case III: Disregarding the possibility of connecting MEG units in the system during the restoration process but exploring the DR program, the restored system has a total in-service active load of 66.77%, to do so, 8 open and 10 closing switching operations are coordinated.

Case IV: This case presents a topology with a total in-service load of 59.29% which requires of 10 open and 10 closing switching operations.

IV. Conclusions

This paper presented a restoration-based approach to address the EDS resilience problem. The problem is formulated as a MILP model that guarantees a finite solution through commercial optimization solvers. The solution of the proposed model provides a recovering plan to minimize the load shedding after a HILP fault event. This recovering plan considers dynamic network reconfiguration, islanding operation, and the scheduling of MEG units. Moreover, a DR program was implemented to maximize the amount of in-service load after a HILP fault event. The obtained results reveal the advantage of considering dynamic network reconfiguration in the restoration process since the more in-service load can be obtained when compared with a restoration process without it. Moreover, the coordination of MEG units is an interesting option to improve the quality of the restoration process. Results also showed that by including a DR program it is possible to increase the amount of in-service load; however, its contribution is lower than the MEGs' one. On the other hand, when the dynamic network reconfiguration is disregarded, the amount of in-service load remains constant throughout the periods. Nevertheless, the obtained results are inferior when compared to cases that consider dynamic network reconfiguration. These results support the need of implementing a restoration process that includes the dynamic network reconfiguration. As for directions of future research, the proposed strategy could be extended to perform a sensitivity analysis to explore the order in which the operational alternatives must be coordinated, considering their availability in the system. In addition, the approach could include new devices to improve the EDS recoverability, i.e., mobile emergency energy storage units and repair crews.

Appendix

This appendix presents the linearization of constraint (4) according to the piecewise approximation presented in [20].

$$\tilde{V}^{SQ}_{j,t,c} I^{SQ}_{ij,t,c} = \sum_{y=1}^{Y} m_{ij,y} \tilde{P}_{ij,t,c,y} + \sum_{y=1}^{Y} m_{ij,y} \tilde{Q}_{ij,t,c,y} \quad (40)$$

$$P_{ij,t,c} = P^{+}_{ij,t,c} - P^{-}_{ij,t,c} \quad (41)$$

$$Q_{ij,t,c} = Q^{+}_{ij,t,c} - Q^{-}_{ij,t,c} \quad (42)$$

$$\sum_{y=1}^{Y} \tilde{P}_{ij,t,c,y} = P^{+}_{ij,t,c} + P^{-}_{ij,t,c} \quad (43)$$

$$\sum_{y=1}^{Y} \tilde{Q}_{ij,t,c,y} = Q^{+}_{ij,t,c} + Q^{-}_{ij,t,c} \quad (44)$$

$$\forall (ij \in \Gamma_B, t \in \Gamma_T, c \in \Gamma^t_C)$$

$$0 \le \tilde{P}_{ij,t,c,y} \le \bar{V}\bar{I}_{ij}/Y \quad (45)$$

$$0 \le \tilde{Q}_{ij,t,c,y} \le \bar{V}\bar{I}_{ij}/Y \quad (46)$$

$$m_{ij,y} = (2\lambda - 1)\bar{V}\bar{I}_{ij}/Y \quad (47)$$

where Y is the number of blocks of the linearization, $m_{ij,y}$ is the slope of the yth block of the power flow through branch ij, and $\tilde{P}_{ij,t,c,y}$ and $\tilde{Q}_{ij,t,c,y}$ are the values of the yth block of $|P_{ij,t,c}|$ and $|Q_{ij,t,c}|$, respectively.

Constraint (40) is a linear representation of the quadratic constraint (4), where the parameter $\tilde{V}^{SQ}_{j,t,c}$ represents the square of the voltage at node j that is set at 1.0 to simplify the formulation.

Constraints (41) and (42) determines the active and reactive power flow through branches, respectively, by using the non-negative variables $P^{+}_{ij,t,c}$, $P^{-}_{ij,t,c}$, $Q^{+}_{ij,t,c}$, and $Q^{-}_{ij,t,c}$. Constraints (43) and (44) determine the values of $\tilde{P}_{ij,t,c,y}$ and $\tilde{Q}_{ij,t,c,y}$ in each block of the discretization, respectively.

Constraints (45)–(47) are used to limit the variables $\tilde{P}_{ij,t,c,y}$ and $\tilde{Q}_{ij,t,c,y}$, and to calculate the values of the parameters $m_{ij,y}$ used in the discretization, respectively.

References

[1] R. J. Campbell, "Weather-related power outages and electric system resiliency," Washington D.C, 2012.

[2] F. H. Jufri, V. Widiputra, and J. Jung, "State-of-the-art review on power grid resilience to extreme weather events: Definitions, frameworks, quantitative assessment methodologies, and enhancement strategies," *Appl. Energy*, vol. 239, pp. 1049–1065, Apr. 2019.

[3] Z. Wang and J. Wang, "Self-healing resilient distribution systems based on sectionalization into microgrids," *IEEE Trans. Power Syst.*, vol. 30, no. 6, pp. 3139–3149, Nov. 2015.

[4] B. Chen, C. Chen, J. Wang, and K. L. Butler-Purry, "Multi-time step service restoration for advanced distribution systems and microgrids," *IEEE Trans. Smart Grid*, vol. 9, no. 6, pp. 6793–6805, Nov. 2018.

[5] S. Lei, C. Chen, Y. Li, and Y. Hou, "Resilient disaster recovery logistics of distribution systems: co-optimize service restoration with repair crew and mobile power source dispatch," *IEEE Trans. Smart Grid*, vol. 10, no. 6, pp. 6187–6202, Nov. 2019.

[6] B. Taheri, A. Safdarian, M. Moeini-Aghtaie, and M. Lehtonen, "Distribution system resilience enhancement via mobile emergency generators," *IEEE Trans. Power Deliv.*, vol. 36, no. 4, pp. 2308–2319, Aug. 2021.

[7] A. K. Erenoğlu and O. Erdinç, "Post-Event restoration strategy for coupled distribution-transportation system utilizing spatiotemporal flexibility of mobile emergency generator and mobile energy storage system," *Electr. Power Syst. Res.*, vol. 199, p. 107432, Oct. 2021.

[8] L. Jiang *et al.*, "Resilient service restoration for distribution systems with mobile resources using Floyd-based network simplification method," *IET Gener. Transm. Distrib.*, pp. 1–16, Sep. 2021.

[9] Q. Zhang, Z. Ma, Y. Zhu, and Z. Wang, "A two-level simulation-assisted sequential distribution system restoration model with frequency dynamics constraints," *IEEE Trans. Smart Grid*, vol. 12, no. 5, pp. 3835–3846, Sep. 2021.

[10] Q. Zhang, Z. Wang, S. Ma, and A. Arif, "Stochastic pre-event preparation for enhancing resilience of distribution systems," *Renew. Sustain. Energy Rev.*, vol. 152, p. 111636, Dec. 2021.

[11] P. Siano, "Demand response and smart grids - A survey," *Renewable and Sustainable Energy Reviews*, vol. 30. Elsevier Ltd, pp. 461–478, 2014.

[12] M. R. Kleinberg, K. Miu, and H. D. Chiang, "Improving service restoration of power distribution systems through load curtailment of in-service customers," *IEEE Trans. Power Syst.*, vol. 26, no. 3, pp. 1110–1117, Aug. 2011.

[13] S. Mousavizadeh, M. R. Haghifam, and M. H. Shariatkhah, "A linear two-stage method for resiliency analysis in distribution systems considering renewable energy and demand response resources," *Appl. Energy*, vol. 211, pp. 443–460, Feb. 2018.

[14] F. Hafiz, B. Chen, C. C. Chen, A. R. De Queiroz, and I. Husain, "Utilising demand response for distribution service restoration to achieve grid resiliency against natural disasters," *IET Gener. Transm. Distrib.*, vol. 13, no. 14, pp. 2942–2950, Jul. 2019.

[15] A. S. Kahnamouei and S. Lotfifard, "Enhancing resilience of distribution networks by coordinating microgrids and demand response programs in service restoration," *IEEE Syst. J.*, pp. 1–12, 2021.

[16] P. Gautam, P. Piya, and R. Karki, "Resilience assessment of distribution systems integrated with distributed energy resources," *IEEE Trans. Sustain. Energy*, vol. 12, no. 1, pp. 338–348, Jan. 2021.

[17] M. A. Gilani, A. Kazemi, and M. Ghasemi, "Distribution system resilience enhancement by microgrid formation considering distributed energy resources," *Energy*, vol. 191, p. 116442, Jan. 2020.

[18] M. Esfahani, N. Amjady, B. Bagheri, and N. D. Hatziargyriou, "Robust resiliency-oriented operation of Active distribution networks considering windstorms," *IEEE Trans. Power Syst.*, vol. 35, no. 5, pp. 3481–3493, Sep. 2020.

[19] J. M. H. Ortiz, O. D. Melgar-Dominguez, M. S. Javadi, S. F. Santos, J. R. S. Mantovani, and J. P. S. Catalao, "Distribution systems resilience improvement utilizing multiple operational resources," in *2021 IEEE International Conference on Environment and Electrical Engineering and 2021 IEEE Industrial and Commercial Power Systems Europe (EEEIC / I&CPS Europe)*, 2021, pp. 1–6.

[20] N. Alguacil, A. L. Motto, and A. J. Conejo, "Transmission expansion planning: A mixed-integer LP approach," *IEEE Trans. Power Syst.*, vol. 18, no. 3, pp. 1070–1077, Aug. 2003.

[21] R. A. Jabr, R. Singh, and B. C. Pal, "Minimum loss network reconfiguration using mixed-integer convex programming," *IEEE Trans. Power Syst.*, vol. 27, no. 2, pp. 1106–1115, May 2012.

[22] M. E. Baran and F. F. Wu, "Network reconfiguration in distribution systems for loss reduction and load balancing," *Power Deliv. IEEE Trans.*, vol. 4, no. 2, pp. 1401–1407, 1989.

[23] C. Su and C. Lee, "Network reconfiguration of distribution systems using improved mixed-integer hybrid differential evolution," *IEEE Trans. Power Deliv.*, vol. 18, no. 3, pp. 1022–1027, 2003.

[24] J. M. Home-Ortiz, M. Pourakbari-Kasmaei, M. Lehtonen, and J. R. Sanches Mantovani, "Optimal location-allocation of storage devices and renewable-based DG in distribution systems," *Electr. Power Syst. Res.*, vol. 172, pp. 11–21, Jul. 2019.

Juan M. Home-Ortiz received the B.S. and M.S. degrees in electrical engineering from the Universidad Tecnológica de Pereira, Colombia, in 2011 and 2014, respectively, and the Ph.D. degree in electrical engineering from the São Paulo State University (UNESP), Ilha Solteira, Brazil, in 2019. Currently, he is carrying out postdoctoral research with UNESP.

During 2020–2021, he was a Postdoctoral Researcher with INESC TEC, Porto, Portugal. His research interests include the development of methods for the optimization, planning, and control, of electrical power systems.

Ozy D. Melgar-Dominguez received the B.Sc. degree in electrical engineering from the National Autonomous University of Honduras (UNAH), Tegucigalpa, Honduras, in 2011, the M.Sc. and Ph.D. degrees in electrical engineering from São Paulo State University (UNESP), Ilha Solteira, Brazil, in 2015 and 2018, respectively. In 2018, he was a Visiting Researcher with Aalto University, Finland, for about four months. From 2019 to 2021, he was a Postdoctoral Researcher at UNESP. He is currently the Head of the Department of Generation Planning at System Operator (ODS), Tegucigalpa. His research interests include the development of methodologies for expansion and operation planning of power systems, integration of renewable energy systems and energy storage systems, environmental issues, and optimization techniques.

Mohammad S. Javadi (Senior Member, IEEE) received the B.Sc. degree from Shahid Chamran University, Ahwaz, Iran, in 2007, the M.Sc. degree in power system from the University of Tehran, in 2009, and the Ph.D. degree in electrical power engineering from Shahid Chamran University, in 2014. He is currently an Associate Professor at IAU, Shiraz, Iran, and also a Researcher at the INESC TEC, Porto, Portugal. His research interests include power system operations and planning, multi-carrier energy systems, islanding operation of active distribution networks, distributed renewable generation, demand response, and smart grid. He received the Best Reviewer Awards from the IEEE Transactions on Smart Grid and the IEEE Transactions on Power System in 2019. Since 2021, he has been serving as an Associate Editor for e-Prime journal.

José Roberto Sanches Mantovani (Member, IEEE) received the B.S. degree from São Paulo State University (UNESP), Ilha Solteira, Brazil, in 1981, and the M.S. and Ph.D. degrees from the University of Campinas, Campinas, Brazil, in 1987 and 1995, respectively, all in electrical engineering. He is currently a full professor with the Department of Electrical Engineering, UNESP.

His research interests include the development of methods for the optimization, planning, and control of electrical power systems, and applications of artificial intelligence in power systems.

João P. S. Catalão (Fellow, IEEE) received the M.Sc. degree from the Instituto Superior Técnico (IST), Lisbon, Portugal, in 2003, and the Ph.D. degree and Habilitation for Full Professor ("Agregação") from the University of Beira Interior (UBI), Covilha, Portugal, in 2007 and 2013, respectively. Currently, he is a Professor at the Faculty of Engineering of the University of Porto (FEUP), Porto, Portugal, and Research Coordinator at INESC TEC. He was the Primary Coordinator of the EU-funded FP7 project SiNGULAR ("Smart and Sustainable Insular Electricity Grids Under Large-Scale Renewable Integration"), a 5.2-million-euro project involving 11 industry partners.

His research interests include power system operations and planning, power system economics and electricity markets, distributed renewable generation, demand response, smart grid, and multi-energy carriers.